ABSORPTION COEFFICIENT AND DIELECTRIC FUNCTION OF DIRECT BAND GAP SILICON NANOCRYSTALLITES

A thesis submitted to the School of Graduate Studies
Addis Ababa University

In partial Fulfilment of the Requirements for the
Degree of Master of Science in Physics

By

Hagos Gebrehiwet

Addis Ababa, Ethiopia
July 2007

ADDIS ABABA UNIVERSITY
FACULTY OF SCIENCE
DEPARTMENT OF PHYSICS

The undersigned hereby certify that they have read and recommended to the Faculty of Science School of Graduate Studies for acceptance a thesis entitled "**Absorption coefficient and dielectric function of direct band gap silicon nanocrystallites**" by in partial fulfillment of the requirements for the degree of **Master of Science in Physics**.

Name	Signature
Dr. S. K. Ghoshal, Advisor	_______________
Dr. Mulugeta B., Examiner	_______________
Dr. H. S. Tewari, Examiner	_______________

To every one who was helpful to me during my Secondary school studies, especially Adhanom Kindeya and Fitsum Gebrehaweria.

Acknowledgements

I would like to thank my advisor as well as instructor Dr. Sib Krishna Ghoshal for his indispensable prompt help and invaluable effort in guiding, supervising, encouraging and providing the necessary materials throughout my graduate study and during the course of this thesis.

I have benefited a lot from physics department graduate computer lab. Therefore, I am very much pleased to thank the department.

It gives me great pleasure to express my great gratitude to World Vision Australia, Members of this organization and world vision Ethiopia for their genuine support for the period of August, 2001- August, 2007.

Of course, I am grateful to my mother, my little sister Amlisha and, my brothers Terefe and Tsegazeab for their patience and *love*. My cousins Gebremedhin and Tesfa-alem (and they know why), deserve gratitude and gratefulness.

Finally, I wish to thank the following: Mahari and Lamenew (for their friendship); Ashenafi, Berihu, Shibeshi and Habtamu (for all the good and bad times we had together).

Addis Ababa, Ethiopia Hagos Gebrehiwet

Abstract

Silicon is an ubiquitous electronic material and the discovery of strong room temperature luminescence from porous silicon in 1990 raised hopes it may find a new lease of life in the emerging field of optoelectronics. First, the luminescence was shown to be emitted from nanostructures in a porous silicon network. Later the same emission was seen from silicon nanocrystallites and the concept of a silicon quantum dot emerged. A number of different models have been proposed for the origin of the light emission. Some involve interface states between a silicon nanocrystallite and a surrounding shell, while others consider the effect of quantum confinement in an indirect bandgap semiconductor.

In order to clarify the influence of morphological properties, such as size or shape, of a silicon nanocrystallite on its optical properties, calculations of optical absorption coefficient and dielectric function of silicon nanocrystallites as a function of effective silicon nanocluster size (diameter) and photon energy were attempted using **k**.**p** method.

To conclude, the work presented in this thesis gives support to the quantum confinement effect in explaining the optical properties of band gap nano-sized silicon below 10nm, as well as highlighting the importance of calculating optical parameters of silicon nanocrystallites to understand optical properties in the luminescence process.

Table of Contents

Table of Contents **vi**

List of Figures **vii**

1 Introduction **1**

1.1 What are silicon nanocrystallites? 1

1.1.1 Applications of silicon nanocrystallites 3

1.1.2 Fabrication of silicon nanocrystallites 6

1.2 Quantum confinement and optical properties 10

1.2.1 Photoluminescence 12

1.2.2 Nonlinear optical properties 16

1.3 Thesis outline 19

2 Band theory and density of states of silicon nanocrystallites **20**

2.1 Density of states 20

2.2 Electron band structure and its modification 23

2.2.1 The **k**.**p** perturbation theory neglecting spin 26

3 Calculation of optical absorption coefficient and dielectric function **30**

3.1 Optical transition rate and dipole matrix elements 30

3.2 Calculation of linear optical absorption 34

3.2.1 The fundamental absorption edge and joint density of states . 36

3.3 Dielectric function 39

4 Results and Discussions **42**

5 Summary and Conclusion **48**

Bibliography **51**

List of Figures

1.1 *Silicon QDs as sensitizers for Erbium: high absorption cross-section of silicon nanocrystallites, their larger bandgap than corresponding inter-level spacing in Er^{3+}, and lower energy backtransfer rate due to spatial decoupling are the main advantages of such a mechanism of Erbium excitation [8].* 5

1.2 *Formation of porous silicon. (Left) SEM image illustrating the three typical etching regimes in silicon: porous formation, transition regime with pillar-like structures, and electropolishing [12]. (Right) TEM micrograph of porous silicon grains with characteristic size of several nanometers [13].* 7

1.3 *Formation of silicon nanocrystallites in a SiO_2 shell by implantation of silicon ions of 270 keV energy into silicon dioxide with subsequent annealing [12].* 8

1.4 *Photoluminescence peak energy of silicon nanocrystallites as a function of crystal size. The solid line was obtained from the effective mass theory for three-dimensionally confined Silicon nanocrystallites [14].* . . 13

1.5 *Room-temperature photoluminescence spectra of silicon nanocrystallites. The peak position can be controlled by appropriate adjustment of the nanocrystallite size [14].* 15

1.6 *The variation of $\chi^{(3)}$ with the silicon nanocrystallite radius (r) in silicon nanocrystallite grown by PEVCD. The dashed curves show the fit to a $\chi^{(3)}_{Si-nc} = \chi^{(3)}_{bulk} + \frac{A}{r} + \frac{B}{r^2}$ dependence [11].* 18

2.1 *Density of states for various geometries of semiconductor materials: (a) 3-D bulk, (b) quantum well, a 2-D structure, (c) quantum wire, a 1-D structure, and (d) quantum dot, a 0-D entity. The dotted line in (a) is the thermal distribution of carriers.* 22

4.1 *Optical absorption coefficient as a function of silicon nanocluster size for photon energy* $\hbar\omega$*=2.2 eV.* 44

4.2 *Optical absorption coefficient as a function of photon energy for effective silicon nanocluster size d=8nm.* 45

4.3 *Imaginary part of the dielectric function as a function of silicon nanocluster size for photon energy* $\hbar\omega$*=2.2 eV.* 46

4.4 *Imaginary part of the dielectric function as a function of photon energy for effective silicon nanocluster size d=8nm.* 47

Chapter 1

Introduction

In this chapter we are going to see what silicon nanocrystallites are, their applications in the real world, some of their fabrication methods and how both the linear and non-linear optical properties of nanostructures get affected by quantum confinement.

1.1 What are silicon nanocrystallites?

A nanocrystal is a crystalline material with dimensions measured in nanometers and a nanoparticle with a structure that is mostly crystalline in the interior. These materials are of huge technological interest since many of their optical, electronic and thermodynamic properties show strong size dependence, and can therefore be controlled through careful manufacturing processes.

Silicon (Si) is the leading material as regards high-density electronic functionality. Integration and economy of scale are the two key ingredients in the technological success of silicon. Its band gap (1.12eV) is ideal for room temperature operation, and its oxide (SiO_2) allows the processing flexibility to place more than 10^8 transistors

on a single chip. The continuous improvements in silicon technology have made it possible to grow and process 300mm wide single silicon crystal at low cost and even larger crystallites are now under development.

Crystalline silicon is the dominant material in microelectronics, but until now it has not been suitable for the realization of active optical devices, due to its poor light emission at room temperature ascribed to a band structure with an indirect gap and a small exciton binding energy.

One of the strategic objectives of the nanotechnology concept is the development of new materials having nanometer sizes which have entirely new physical properties and, therefore, new functionality. Historically, nanostructured silicon was first produced by Ingeborg and Arthur Uhlir at Bell Labs in the 1950s [1]. They were studying electropolishing of silicon surfaces using aqueous solutions of HF and found that, at low current densities, it results in a sponge-like structure. In the 1970s, researches revealed the porous nature of the material, but intended to use it only as a precursor for making low dielectric constant layers. Despite the observation of photoluminescence from porous silicon (PS) at cryogenic temperatures in 1984, wide attention to optical properties of porous silicon and other nanosilicon-containing systems was drawn only after reports on visible light emission at room temperature by Canham and blue shift of the absorption by Lehmann and Gsele in 1990 [2].

In silicon science and technology the desire for the integration of optoelectronic devices with silicon microelectronics has led to the search for silicon-based structures that emit light with a high quantum efficiency value. Among the different approaches used by researchers, the most recent is the fabrication of silicon nanostructures (porous

silicon, quantum dots, quantum wells, nanoclusters), which exhibit strong room temperature photoluminescence [3]. This emission is observed only after a drastic size reduction of silicon and has been related to a quantum confinement effect that occurs only when the particle size is smaller than the exciton radius in bulk silicon (∼5nm). The quantum confinement widens the band gap and extends the wavefunction in the momentum space, relaxing the k-selection rules [4, 5]. The k-selection rules imply the conservation of momentum in both direct and indirect bandgap semiconductors.

There are two different mechanisms to study for the electron-hole radiative recombination: the first assumes that the recombination occurs across the nanostructured gap, the other hypothesizes that the electron excited across the widened gap relaxes in the low-lying energy surface states [6, 7]. In the latter case a small photoluminescence peak energy shift with the particle size is observed, whereas in the other case the band gap energy scales as an inverse power of particle diameter. Next section focus on major applications.

1.1.1 Applications of silicon nanocrystallites

The low-dimensional semiconductor structures are of high interest due to the significant technological implications in optics and nanoelectronics. The wide interest in nanosolid or porous silicon (PS) resulted primarily from the proposal, in 1990, that efficient visible light emission from high porosity structures. However, nanoscale silicon is a complex material with regard to its stability, because its optical properties show environmental and ageing degradation with resulting ambiguity in device

performance evaluation. People usually approach to overcome these difficulties by incorporating the light-emitting silicon nanoparticles inside an appropriate matrix material that exhibits both chemical inertness and a band gap suitable for quantum confinement, for example polycrystalline diamond [3].

Silicon nanocrystallites have tremendous applications in photoluminescence, opto-electronic and photonic devices. They can be easily integrated into silicon wafer processing and utilized for biological and chemical sensing, potential applications in silicon-based optoelectronic integrated circuits or for light-emitting devices, optical sensors, photo sensors and memory devices. For example, silicon quantum dots used as sensitizer for Erbium [Fig.(1.1)]. Silicon nanocrystallites can be used for optical communication technology to develop photonic integrated circuits: optical chips in which optical signals are guided, split, switched, multiplexed or amplified. Polarization-sensitive linear and nonlinear photonic elements based on birefringent nanostructured silicon can be fabricated.

The high integration levels reached by the silicon microelectronic industry in the nanometer range have permitted a whole electronic system to be included on a single chip (the system-on-chip (SoC) approach). This yields incredible processing capability and high-speed device performance. For example, in addition to light emission, porous silicon (PS) due to its remarkable structural properties and morphology in conjunction with the ability to tailor its surface chemistry have led to completely new applications, such as chemical and biological sensing, fuel cells, photosynthesis [9], drug delivery [2], explosives [10], adsorbers etc. Nanosilicon-based explosives oxidizer filled porous silicon layers have a morphology completely different from ordinary high explosives.

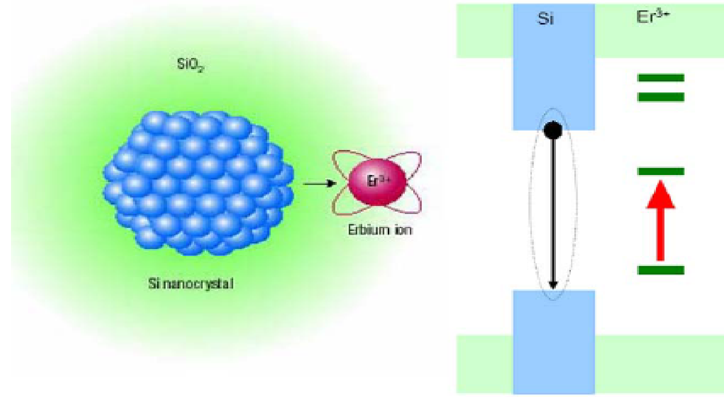

Figure 1.1: *Silicon QDs as sensitizers for Erbium: high absorption cross-section of silicon nanocrystallites, their larger bandgap than corresponding interlevel spacing in* Er^{3+}*, and lower energy backtransfer rate due to spatial decoupling are the main advantages of such a mechanism of Erbium excitation [8].*

This explosive system reveals a variety of new possible applications in different fields, e.g. as a novel, very fast airbag initiator. Unfortunately, all of the currently available production methods provide a low yield of silicon nanocrystallites while most of the applications in various fields require large quantities of nanostructured silicon. To have large scale production, fabrication issue is important and therefore, we discuss it briefly in the next subsection.

1.1.2 Fabrication of silicon nanocrystallites

Silicon nanostructures are produced in different ways. Silicon nanocrystallites are generally fabricated by the precipitation of excess silicon in silicon-rich oxides (SRO) which are produced either during deposition, using techniques such as plasma-enhanced chemical vapour deposition (PECVD), or subsequent to the growth of a stoichiometric SiO_2 layer by ion-implantation of silicon [3]. Typically, silicon nanocrystallites are obtained by the post annealing of a silicon-rich silicon oxide at 1100^oC. Silicon nanocrystallites can also be prepared by reactive silicon deposition onto quartz, by plasma enhanced chemical vapor deposition, by magneton sputtering or by an aerosol procedure [11]. Recently, laser pyrolysis technique has been introduced to achieve relatively narrow size distribution of silicon nanocrystals [2]. Let us see some of the methods in detail.

1.1.2.1 Preparation of porous silicon

Porous silicon (PS), whose structural investigations have confirmed that it consists of silicon nanocrystal assemblies of different size (typically a few nm) and shape, is formed by electrochemical anodization of bulk silicon in an HF electrolyte [Fig.(1.2)]. The solution employed is typically aqueous 50 percent HF mixed with ethanol. The electrical source chosen for the process is usually current controlled, because the current density and the porosity are directly related. The anodization reaction at the Si/electrolyte interface requires the presence of holes [11]. Therefore, the natural choice for substrate doping is P-type. However, n-type substrates can also be employed for porous silicon fabrication, provided that generation mechanism for excess

holes are available- for example, by using light beam, or by biasing the substrate in the breakdown regime.

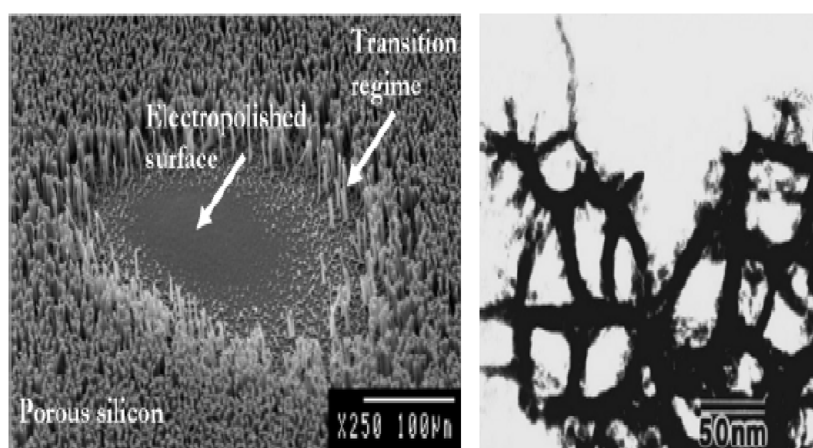

Figure 1.2: *Formation of porous silicon. (Left) SEM image illustrating the three typical etching regimes in silicon: porous formation, transition regime with pillar-like structures, and electropolishing [12]. (Right) TEM micrograph of porous silicon grains with characteristic size of several nanometers [13].*

Depending on the type of doping (p- or n-types) and the doping level of the wafer the sizes of pores and remaining silicon crystallites can be varied from micrometers to nanometers. Porous silicon fabricated on lightly p-type-doped substrates has an average nanocrystal size of 2-5 nm. Since the exciton Bohr radius of silicon is around 4.3 nm, quantum confinement effects and in particular, large values of photoluminescence (PL) efficiency are especially evident in this type of porous silicon. On the other hand, in highly p-type-doped wafer (i.e with typical resistivity values around 0.01 Ωcm), the size of the pores and structures is of the order of 10 nm. The quantum confinement effects are in this case less important, thus explaining why the Photoluminescence emission is remarkably more weak in low-resistivity porous silicon. However, carrier

transport can be turned over a much wider range, and larger porosity ranges can be obtained. This preparation procedure has attracted much interest due to its simplicity, different from costly litho-graphic or epitaxial techniques that were at the time the conventional approaches to realize nanosized semiconductor [11].

1.1.2.2 Ion-implanted silicon nanocrystallites

As the internal surface of porous silicon is enormous, it is also very reactive. This makes porous silicon very interesting for sensor applications but it is a problem when porous silicon is used in photonic devices. Thus alternative techniques have been developed to produce silicon nanocrystallite (Si-nc). Ion-implanted silicon nanocrystallite can be obtained by implanting silicon into silicon wafers or SiO_2 substrates (quartz or thermally grown oxide) and by annealing the samples [Fig.(1.3)].

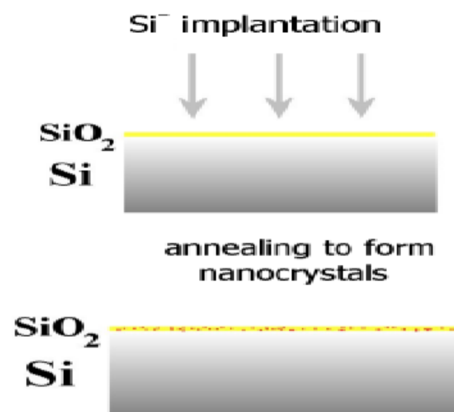

Figure 1.3: *Formation of silicon nanocrystallites in a SiO_2 shell by implantation of silicon ions of 270 keV energy into silicon dioxide with subsequent annealing [12].*

In contrast to porous silicon, implanted silicon nanocrystallites are very stable and form a reproducible system fully compatible with VLSI technology. The presence of a high-quality SiO_2 matrix guarantees superior oxygen passivation of silicon-related dangling bonds and non-radiative centers. In addition, the interface between the silicon nanocrystallite surface and the SiO_2 matrix can play an active and crucial role in the radiative recombination mechanism. The silicon nanocrystallite region has an effective refractive index, $n_{eff} = 1.71$, larger than that of SiO_2 [11]. Figure [fig.(1.3)] below shows the formation of silicon nanocrystallites in a SiO_2 shell by implantation of silicon ions into SiO_2 with subsequent annealing.

1.1.2.3 Plasma Enhanced Chemical Vapor Deposition (PECVD)-grown silicon nanocrystallites

Silicon nanocrystallites can be also formed by high-temperature annealing of substoichiometric SiO_2 thin films deposited by plasma enhanced chemical vapor deposition (PECVD). In this technique, the desired flow of ratio of high-purity source gases SiH_4 and N_2O is controlled to produce excess silicon content in substoichiometric SiO_2 thin films at a pressure of 10^{-2} Torr. After the depositon, the SiO_x films are annealed at high temperatures under a nitrogen atmosphere. Thermal annealing of SiO_x films leads to the separation of the SiO_x phase into silicon and SiO_2, and silicon nanocrystallite embedded in a SiO_2 matrix are formed [11]. Silicon nanocrystallites embedded in a silicon oxide matrix have a potential for applications in silicon-based optoelectronic devices.The method described here is desirable in terms of integrating silicon based optoelectronic components [14].

Finally, silicon nanocrystallites can also be synthesized by laser-induced decomposition of silane in a gas flow reactor. This technique provides a unique opportunity to fabricate nanosilicon grains whose size is scalable and can be controlled by the reaction parameters in a reproducible way. The silicon nanoparticles will be produced by continuous wave CO_2 laser heating of SiH_4He mixtures in a gas flow reactor. By changing the ratio between SiH_4 and He it was possible to obtain particles with sizes in the 350nm range [3].

1.2 Quantum confinement and optical properties

Over recent years, nanostructuring of semiconductors has been considered as an alternative way to the search for new materials. Material properties, especially optical ones can be modified simply by reducing the dimensions or by proper engineering of macroscopic structures on the nanometer scale. In fact, low dimensional silicon shows light amplification characteristics, non-linear optical effects, photon confinement in both one and two dimensions, photon trapping with evidence of light localization and gas-sensing properties [11].

Due to its indirect band-gap electronic structure, bulk silicon is a very inefficient light emitter. In recent years most research efforts have been directed towards developing different approaches to improve the efficiency of light emission from nanosilicon-based structures. The key idea is that the reduction of the size of silicon nanocrystallites results, due to quantum size effects, in a widely tuneable confinement energy of excitons and a partial breaking of its indirect bandgap nature [15].

The influence of quantum confinement on the optical properties of semiconductor nanocrystallites has been intensively investigated in recent years [16, 17]. In direct band-gap semiconductors both absorption and emission are governed by the fundamental direct gap. Therefore most properties of nanocrystallites can be predicted by relatively simple effective- mass calculations based on known parameters of the band edge states. Spectroscopic studies have revealed an increase of the band gap and the oscillator strength with decreasing size and an atomic-like discrete character of the electronic states in quantum dots [18]. The direct electronic band structure of II-VI and III-V semiconductor quantum dots and the advances in their synthesis and size selection have made them a perfect model system for spectroscopic studies of confinement effects.

The electronic states of silicon nanocrystallites (Si-nc) as compared to that of bulk silicon are dramatically influenced both by quantum confinement (QC) and by the enhanced role of state- and defects-at the surface. The effect of quantum confinement is a rearrangement of the density of electronic states in energy as direct consequence of volume shrinking in one, two or even three dimensions, which can be obtained, respectively, in quantum wells, wires, and dots. On the other hand, the arrangement of the atomic bonds at the surface also strongly affects the energy distribution of electronic states, since in silicon nanocrystallites the silicon atoms are either at the surface or a few lattice sites away. The quantum confinement and a suitable arrangement of interfacial atomic bond can provide in silicon nanocrystallites radiative recombination efficiencies that are orders of magnitude larger than in bulk silicon, significant optical non-linearity and even optical gain [3, 19].

1.2.1 Photoluminescence

The optical properties of bulk silicon are mediocre because the light-emission in the bulk is a phonon-assisted indirect process. Therefore, to improve on the light-emission feature in silicon-based materials is a challenge for both technological and fundamental research.

Silicon nanocrystallites (nc-Si) with diameters, d, less than ∼5nm exhibit room temperature photoluminescence (PL) [20] due to the recombination of quantum confined excitons [21] which is a result of a significant overlap in electron and hole wavefunctions. Since the strength of the luminescence (i.e, the emission rate and quantum efficiency) depends on the extent of this overlap and the transition probability, a possible means for increasing this overlap for the silicon-based materials may be accomplished through, for example, alloying to change the band structure, introducing impurities to produce the intermediate state through which the hole, or zone folding to yield the desired quasidirect transition.

According to their surface termination, silicon nanocrystallites can be classified into categories: hydrogen or oxygen terminated. Nanocrystallites of freshly prepared porous silicon belong to the first category, whereas the later category contains aged and oxidized-surface porous silicon and silicon nanocrystallites embedded in SiO_2 thin films. For H-terminated, photoluminescence spectral shows continuous shift of peak energy from the bulk band gap to the visible region with a good agreement with the quantum confinement effect, whereas the photoluminescence spectra of oxidized-surface porous silicon are confined to a specific region [19].

Generally, silicon nanocrystallites grown by different methods exhibit strong photoluminescence in the red region and progressively shift towards the blue when the mean size decreases. Depending on the size, the photoluminescence of silicon nanocrystals can be tuned from the near infrared (1.38 eV) to the ultraviolet (3.02 eV) i.e as the size of a silicon nanocrystallite structure decreases, the band gap of the material increases due to the quantum confinement effect [Fig.(1.4)].

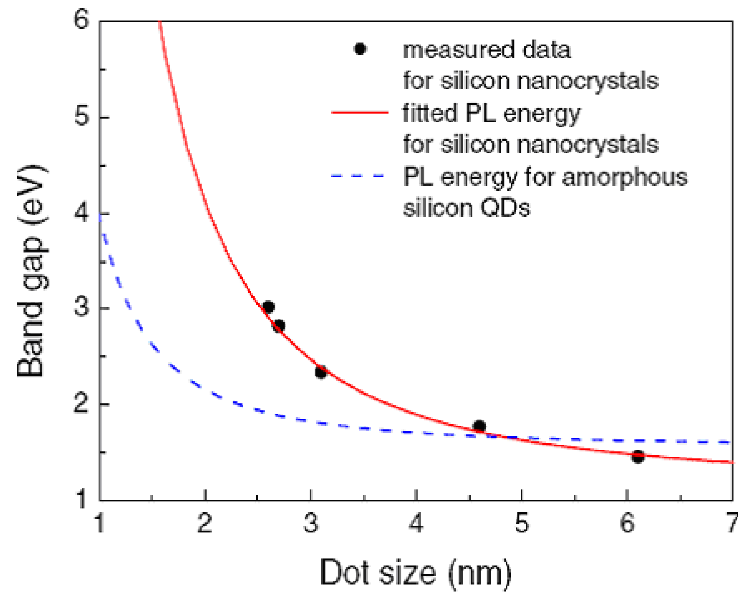

Figure 1.4: *Photoluminescence peak energy of silicon nanocrystallites as a function of crystal size. The solid line was obtained from the effective mass theory for three-dimensionally confined Silicon nanocrystallites [14].*

A blue shift in optical luminescence is the result of quantum confinement effect. Similarly the edge absorption spectra also shifts towards the blue with decrease of the silicon nanocrystallites size. However, a quantitative discrepancy between the energy of photoluminescence and the optical band gap calculated from the quantum confinement theory exists.

For example, a number of groups have reported that when the crystallite size of silicon nanostructures in a silicon oxide matrix is controlled, the experimental photoluminescence energies in air are not in good agreement with values that are theoretically calculated from quantum confinement effects [17, 18]. Wolkin et al. proposed that oxygen is related to the trapping of an electron (or even an exciton) by silicon-oxygen double bonds and produces localized levels in the bandgap of nanocrystallites [19].

Therefore, a quantum confinement effect is not in good agreement with the theoretical calculation in silicon nanostructures, after exposure to air [22]. Even when a silicon oxide is used as a typical matrix material that hosts silicon nanostructures, a silicon oxide matrix may not provide an appropriate emission state for a quantum confinement effect in small silicon crystallites. Because of this, people focus on choosing an appropriate matrix material for silicon nanocrystallites at present [12].

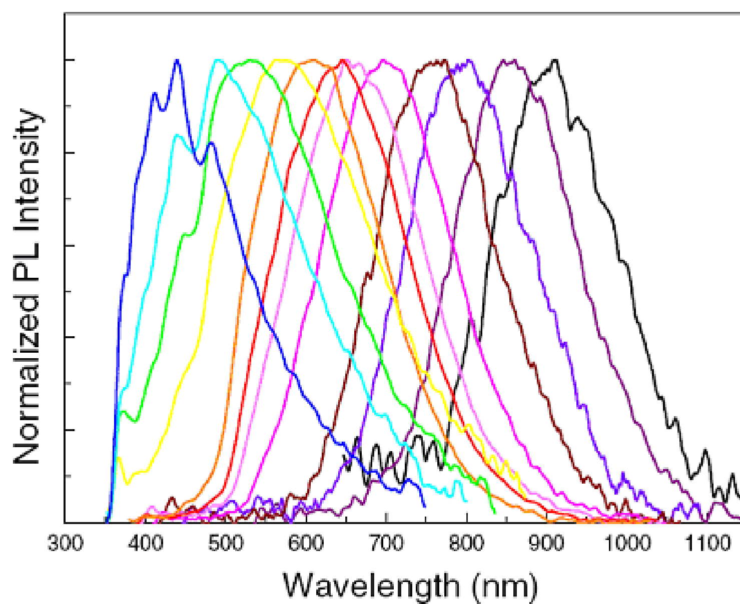

Figure 1.5: *Room-temperature photoluminescence spectra of silicon nanocrystallites. The peak position can be controlled by appropriate adjustment of the nanocrystallite size [14].*

Figure 1.5 shows a room-temperature photoluminescence spectrum obtained from various sized silicon nanocrystals, where the tuning of the photoluminescence emission from 410 to 900 nm is possible by controlling the size of the silicon nanocrystallite and, as a result, the emission color can be changed by controlling the size of the nanocrystallite. For example, nanocrystallite sizes corresponding to red, green, and blue emission are 4.6, 3.1, 2.7 nm, respectively.

1.2.2 Nonlinear optical properties

One of the most important properties of the nanocrystallite assemblies is their strong nonlinear optical response. Nonlinear optical effects such as dynamic and persistent bleaching of absorption have been observed due to the fact that presence of the first photoexcited electron-hole (eh) pair modifies the energy and oscillator strength of the following absorption events. Much stronger nonlinear effects can be seen in the emission from nanocrystallite ensembles. The main reason for this is the high rate of Auger processes in nanocrystallites. In a bulk semiconductor the efficiency of this process is restricted by the conservation of the total momentum to compensate the final large momentum of the fast electron (hole) at low temperatures a phonon has to be emitted. This scenario is very similar to that for indirect optical transitions [13].

Besides the linear optical properties, non-linear optical properties of silicon nanocrystallites are also of major interest because they are also promising materials for non-linear optical applications like for photonic device applications such as in all-optical switching. Intensity dependent changes in optical properties are prominent at high intensities (I) of a pump laser, particularly third order non-linear effects. Numerous reports are available on the nonlinear optical properties of silicon nanocrystallites by using porous silicon and silicon nanocrystallites prepared by sol-gel, laser ablation, ion-implanted, and PEVCD techniques, but a more systematic study of well-defined systems is required, particularly to elucidate the role of quantum confinement and interface states [11].

Non-linear optical behavior can be characterized in terms of non-linear susceptibility. Though the imaginary part of second- ($\Im\chi^{(2)}$) and the third-order ($\Im\chi^{(3)}$) susceptibilities are the most important ones, second-order ($\Im\chi^{(2)}$) is zero because all even power susceptibilities are zero for crystals having a point group with a center symmetry or for glasses which are structurally isotropic. So the most important non-linear ($\Im\chi^{(3)}$) susceptibility in silicon nanocrystallites is the third-order one.

Third-order non-linear effects are generally characterized by the non-linear absorption (β) and non-linear refractive index (γ). The non-linear coefficients, namely (β) and (γ), are described by $\alpha(I) = \alpha_0 + (\beta)I$ and $n(I) = n_0 + (\gamma)I$ where α_0 and n_0 stand for the linear absorption and refractive index respectively. The β- and γ-values are used to evaluate the imaginary ($\Im\chi^{(3)}$) and real($\Re\chi^{(3)}$) parts of the third-order non-linear susceptibility using $\Re\chi^{(3)} = 2n_0^2\epsilon_0 c\gamma$ and $\Im\chi^{(3)} = \frac{2n_0^2\epsilon_0 c\lambda\beta}{2\pi}$, where ϵ_0 is the permittivity of free space, λ is wavelength and c is the velocity of light.

The non-linear absorption in most of the refractive materials arises from either direct multiphonon absorption or saturation of single-photon absorption. It is interesting to note that the non-linear absorption in silicon nanocrystallites formed by ion-implantation and laser ablation is selective as regards the excitation as well as cluster size. For example, laser-ablated samples exhibit saturation of absorption and bleaching effects (change of sign of the non-linear absorption from positive to negative with the increase of the pump intensity) at near-resonant excitations (355 and 532 nm). In contrast, ion-implanted samples show an almost linear dependence of β on the pump power, clear evidence of two-phonon non-linear process [11].

It is found that $\Re\chi^{(3)} \gg \Im\chi^{(3)}$ which show us the non-linearity is mostly refractive.

The absolute values of $\chi^{(3)} = ((\Re\chi^{(3)})^2 + (\Im\chi^{(3)})^2)^{\frac{1}{2}}$ of silicon nanocrystallites are significantly larger than that of the bulk silicon values and the same orders of magnitude as those for porous silicon [23, 24]. The increase in $\chi^{(3)}$ with respect to bulk values in low-dimensional semiconductors is mainly attributed due to the quantum confinement effects because intraband transitions are expected to be size dependent as they originated from modified electronic transitions [25, 26].

The quantum confinement effects on $\chi^{(3)}$ have been estimated in several works [25, 26, 27]. Theoretical attempts were made to study porous silicon as one dimensional quantum wire and for non-resonant excitation conditions [25, 26]. It was found that the increase in the oscillator strengths caused by the confinement-induced localization of excitons give rise to the increase of $\chi^{(3)}$ and it is given with respect to bulk as $\chi^{(3)}_{Si-nc} = \chi^{(3)}_{bulk} + \frac{A}{r} + \frac{B}{r^2}$ [Fig.(1.6)].

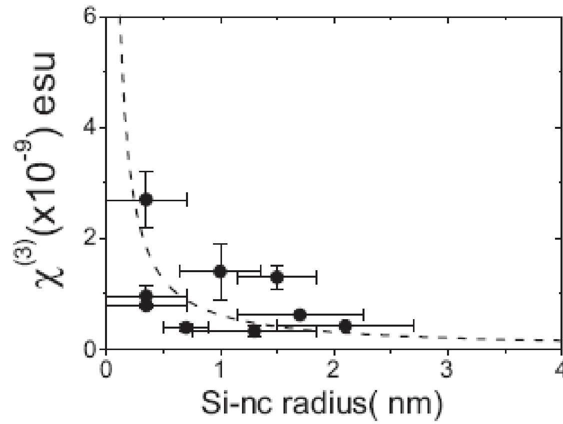

Figure 1.6: *The variation of* $\chi^{(3)}$ *with the silicon nanocrystallite radius (r) in silicon nanocrystallite grown by PEVCD. The dashed curves show the fit to a* $\chi^{(3)}_{Si-nc} = \chi^{(3)}_{bulk} + \frac{A}{r} + \frac{B}{r^2}$ *dependence [11].*

1.3 Thesis outline

In this thesis we study the optical properties of silicon nanoclusters by determining optical absorption coefficient and dielectric function near the band edge as a function of photon energy and size distribution. For this study we have focused on the direct band gap silicon nanoclusters where zero phonon transitions occur. The thesis is organized into five chapters. Chapter 2 discusses the density of states of confined systems and band theory of direct band gap silicon nanoclusters using **k**.**p** method. Chapter 3 discusses how the optical absorption coefficient and dielectric function is related to the band gap and photon energy of the silicon nanoclusters. We found dipole matrix elements of HOMO-LUMO states of silicon nanoclusters using the Kane approximation method to calculate the momentum matrix element for direct band gap semiconductors. In our calculation of the optical absorption coefficient and dielectric function silicon nanoclusters we use the joint density of states together with dipole matrix elements of the HOMO-LUMO states. Chapter 4 contains the result and discussion, and chapter 5 gives the summary and conclusion

Chapter 2

Band theory and density of states of silicon nanocrystallites

In this chapter we are going to discuss how the band theory and the density of states vary as we go from bulk to silicon nanocrystalline quantum structure i.e the electron density of states of a quantum dot (0D), quantum wire (1D), quantum well (2D) and bulk silicon (3D). Finally, we are going to exploit $\mathbf{k}.\mathbf{p}$ perturbation theory for calculation of momentum matrix elements and energy eigenvalue of semiconductors nanostructures in general.

2.1 Density of states

In order to characterize the physical properties like optical transitions, charge transport etc., the information about the density of states is very crucial [28]. The density of states depends on the dimensionality of the system and the energy versus the corresponding wavevector dispersion relation for the system at hand [29].

A general expression for the density of states valid for all types of materials is as a sum delta functions

$$g(E) = \sum_{E_i} \delta(E - E_i), \tag{2.1.1}$$

or

$$g(\omega) = \sum_{k} \delta(\omega - \omega_k). \tag{2.1.2}$$

For parabolic approximation of the energy versus the corresponding wavevector dispersion relation for the electron or hole we can take a simpler form. Therefore, for a three-dimensional bulk material, the DOS is defined as the number of available electronic states per unit volume per unit energy at energy E and is given by

$$g(E) = \frac{\sqrt{2} m_e^{3/2}}{\pi^2 \hbar^3} E^{1/2}. \tag{2.1.3}$$

Passing from three-dimensional bulk to two-dimensional structures, (so called quantum well) the carrier movement is restricted to a plane. Such two-dimensional systems include thin films, layer structures and superlattices. Now the DOS is modified to the number of available electronic states per unit area per unit energy and is given by

$$g(E) = \frac{m_e}{\pi^2 \hbar^2}. \tag{2.1.4}$$

Further reduction in the dimensionality of the system ends up in a quantum wire. Examples of such one-dimensional structures include nanotubes, semiconductor nanowires, and nanorods. For a quantum wire the DOS is defined as the availability of electronic states per unit length per unit energy and is given by

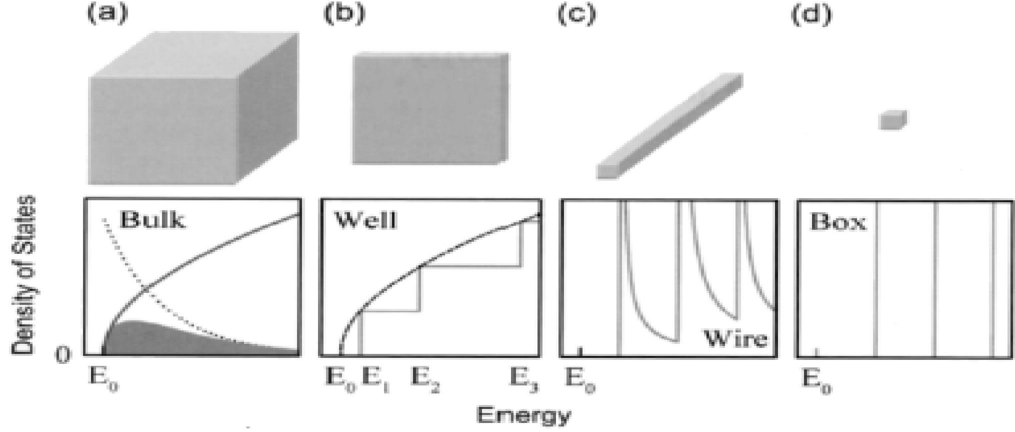

Figure 2.1: *Density of states for various geometries of semiconductor materials: (a) 3-D bulk, (b) quantum well, a 2-D structure, (c) quantum wire, a 1-D structure, and (d) quantum dot, a 0-D entity. The dotted line in (a) is the thermal distribution of carriers.*

$$g(E) = \frac{\sqrt{2}m_e^{1/2}}{\pi\hbar}E^{-1/2}. \tag{2.1.5}$$

Finally, for a zero dimensional system (QD), the confinement is along all three dimensions and the DOS becomes a delta function. Figure (2.1) schematically shows the modifications in the DOS as a function of dimension.

Transformation from a 3-D bulk system to a 2-D thin film changes the DOS from a continuous parabolic dependence to a step like dependence. This is due to the quantization of carrier motion in the thickness direction. Consequently the optical absorption edge is shifted to higher energy with respect to the bulk and above the absorption edge; the spectrum is stepped rather than smooth [30].

2.2 Electron band structure and its modification

Optical transitions in atoms and molecules occur between discrete levels. Semiconductors (bulk) are however characterized by bands and the study of optical processes in semiconductors invariably requires complete knowledge of band structure [31]. The band theory of solids, including semiconductors, is a many-particle theory involving all electrons and ions and their mutual interactions. This many-body problem may be reduced under various approximations to a single-electron problem that predicts most of the important features. In the one electron theory an electron is assumed to exist in a periodic potential and the solution of Schrödinger's equation with periodic boundary conditions yields different bands that are separated from each other by a forbidden bandgap.

We note that in optical transitions from the valence band to the conduction band the electrons involved cover an energy interval of a small fraction of an electron Volt (eV). Therefore, it is sufficient to know the band structure within a few $k_B T$ from the conduction and valence band extrema. For most of the common semiconductors the wavefunctions of the electrons at the band edges are readily describable by atomic **s** and **p** functions. For states slightly away from the extrema the **k**.**p** perturbation theory proves to be a very useful approximation. Therefore, we are going to see expressions for the wavefunctions and effective masses for electrons and holes using **k**.**p** method. For silicon nanostructures states near the extremum of HOMO-LUMO are important and **k**.**p** method we believe should work and we are the first one to put effort in this direction.

A solid consists of many atoms and electrons. The total energy of the system is therefore the sum of the kinetic energies of all the nuclei and the electrons, the potential energies due to internuclear forces, the potential energies of electrons in the field of the nuclei, the potential energy due to the electron-electron interaction, and the magnetic energy associated with the spin and the orbit. The total Hamiltonian of the system may be constructed accordingly. The formidable problem of solving the resultant Schrödinger equation is bypassed invoking several approximations. Since the motion of of the nuclei is sluggish, the electrons instantaneously adjust their motion to that of the ions. The total wavefunction is then written as a product of the wavefunction for ions $\phi(\mathbf{R})$ and that for all electrons $\varphi(\mathbf{r}, \mathbf{R})$ instantaneously dependent on the ionic position $\mathbf{R}$. Introduction of the adiabatic approximation then decouples the Schrödinger equations into a purely ionic equation

$$H_L \phi(\mathbf{R}) = E_L \phi(\mathbf{R}), \tag{2.2.1}$$

and purely electronic equation

$$H_e \varphi(\mathbf{r}, \mathbf{R}) = E_e \varphi(\mathbf{r}, \mathbf{R}), \tag{2.2.2}$$

here $\mathbf{r}$ denoting the electronic coordinates.

The electron potential energy is due to the electron-electron and electron-ion interactions. If the first is considered as a suitable average, so that a constant repulsive contribution is added to the electron energy, each electron becomes independent. The one-electron Schrödinger equation is then,

$$H_{ei} \varphi_i(\mathbf{r}_i, \mathbf{R}) = E_{ei} \varphi_i(\mathbf{r}_i, \mathbf{R}), \tag{2.2.3}$$

where

$$H_{ei} = \frac{\mathbf{p}_i^2}{2m_0} + \sum_i V(\mathbf{r}_i - \mathbf{R}_i), \qquad (2.2.4)$$

and $\mathbf{p}_i$ is the momentum of the ith electron. The Hamiltonian still depends on the fluctuating position of the ion. In the approximation the ions are assumed to lie in their equilibrium position and the effect of ionic vibration is taken as a perturbation. Thus the problem reduces to solving the equation

$$\left[\frac{\mathbf{p}^2}{2m_0} + \sum_i V(\mathbf{r} - \mathbf{R}_{ie})\right]\varphi(\mathbf{r}) = E\varphi(\mathbf{r}). \qquad (2.2.5)$$

The ionic potential V is periodic and the eigenfunction is a Bloch function expressed as

$$\varphi_{n\mathbf{k}}(\mathbf{r}) = u_{n\mathbf{k}}(\mathbf{r})\exp(i\mathbf{k}.\mathbf{r}), \qquad (2.2.6)$$

where the cell periodic part $u_k(\mathbf{r})$ obeys the relation

$$u_{\mathbf{k}}(\mathbf{r} + \mathbf{R}) \simeq u_{\mathbf{k}}(\mathbf{r}). \qquad (2.2.7)$$

In eq.(2.2.5)-(2.2.7) $\mathbf{R}$ is a vector of the Bravais lattice, n denotes the band index and $\mathbf{k}$ is a wave vector of the electron in the first Brillouin zone. From eq.(2.2.6) and eq.(2.2.7)

$$\varphi_{n\mathbf{k}}(\mathbf{r}) \simeq \varphi_{n\mathbf{k}}(\mathbf{r} + \mathbf{R}). \qquad (2.2.8)$$

The Bloch wavefunctions are eigenfunctions of the one-electron Schrödinger equation and therefore they are orthogonal to one another. Thus

$$\int \varphi_{n'\mathbf{k}'}\varphi_{n\mathbf{k}} = \delta_{n'n}\delta_{\mathbf{k}'\mathbf{k}}. \qquad (2.2.9)$$

The wavefunctions are also normalized over the volume V of the crystal and therefore

$$\varphi_{n\mathbf{k}} = V^{-1/3}u_{n\mathbf{k}}(\mathbf{r})\exp(i\mathbf{k}.\mathbf{r}). \qquad (2.2.10)$$

2.2.1 The k.p perturbation theory neglecting spin

The **k**.**p** perturbation theory is based on the fact that the cell periodic part $u_{\mathbf{k}}$ of the electrons, for any value of **k** but different bands, form a complete set. Let us consider the wavefunction for the electrons having a value **k** near the minima in the nth band. For simplicity we assume that the minima are located at **k**=0. This approximation is possible for nano-silicon because due to quantum confinement effect it makes a transition from indirect to direct band gap structure. The theory is applicable also within the minima that are located at $\mathbf{k} = \mathbf{k}_0$. The wavefunction is given by

$$\varphi = u_{n\mathbf{k}}(\mathbf{r}) \exp(i\mathbf{k}.\mathbf{r}) = \left[\Sigma_m C_n u_{m0}(\mathbf{r})\right] \exp(i\mathbf{k}.\mathbf{r}), \tag{2.2.11}$$

since u_{m0} forms a complete orthonormal set. Using this form of φ in the Schrödinger equation one obtains

$$\left[-\frac{\hbar^2}{2m_0}\nabla^2 + \frac{\hbar}{m_0}\mathbf{k}.\mathbf{p} + \frac{\hbar^2 k^2}{2m_0} + V(\mathbf{r})\right] u_{n\mathbf{k}}(\mathbf{r}) = E_{n\mathbf{k}} u_{n\mathbf{k}}(\mathbf{r}). \tag{2.2.12}$$

However u_{m0} is the wavefunction for **k**=0 in the nth band satisfying the equation

$$\left[-\frac{\hbar^2}{2m_0}\nabla^2 + V(\mathbf{r})\right] u_{m0}(\mathbf{r}) = E_m(0) u_{m0}(\mathbf{r}). \tag{2.2.13}$$

We now put eq.(2.2.11) in eq.(2.2.12) and use eq.(2.2.13) to obtain

$$\sum C_m \left[E_m(0) + \frac{\hbar^2}{2m_0}k^2 + \frac{\hbar}{m_0}\mathbf{k}.\mathbf{p}\right] u_{m0}(\mathbf{r}) = \sum C_m E_n(\mathbf{k}) u_{m0}(\mathbf{r}) \tag{2.2.14}$$

Multiplying both sides of eq.(2.2.14) by $u^*_{l0}(\mathbf{r})$ and integrating over the unit cell (V_c), the following set of linear homogeneous equation is obtained

$$C_l \left[E_n(\mathbf{k}) - E_l(0) - \frac{\hbar^2}{2m_0}k^2\right] - \sum_m C_m \frac{\hbar}{m_0}(\mathbf{k}.\mathbf{M}_{lm}) = 0, \tag{2.2.15}$$

where

$$\mathbf{M}_{lm}(0) = \int_{V_c} u^*_{l0}(\mathbf{r})\mathbf{p}u_{m0}(\mathbf{r})d(\mathbf{r}). \tag{2.2.16}$$

By giving l successive integer values one obtains the full set of equations.

In the general case, the set of equations has a non-trivial solution if the determinant of the coefficients C_l is zero. This condition gives the energy eigenvalues $E_n(\mathbf{k})$ in terms of the quantities $E_m(0)$ and $\mathbf{p}_{lm}$. The relative values of the expansion co-efficient C_m are then obtained by using the values $E_n(\mathbf{k})$. The absolute values of C_m are obtained by imposing normalization condition on φ. Therefore, the energy eigenvalues near a characteristic point $\mathbf{k} = 0$ can be expressed as

$$E_n(\mathbf{k}) = E_n(0) + \frac{\hbar^2 k^2}{2m_0} + \frac{\hbar^2}{m_0^2}\sum_{l,n}{}' \frac{[\mathbf{k}.\mathbf{M}_{ln}(0)]^2}{E_n(0) - E_l(0)} \tag{2.2.17}$$

where the prime at the sum indicates summation overall n and l with n$\neq l$.

The second and third terms in eq.(2.2.12) can be developed as small perturbations in the vicinity of the minima $\mathbf{k} = \mathbf{k}_0 \neq 0$. Therefore, eq.(2.2.12) can be written as

$$\left[-\frac{\hbar^2}{2m_0}\nabla^2 + \frac{\hbar}{m_0}(\mathbf{k} - \mathbf{k}_0).\mathbf{p} + \frac{\hbar^2(\mathbf{k} - \mathbf{k}_0)^2}{2m_0} + V(\mathbf{r})\right]u_{n\mathbf{k}}(\mathbf{r}) = E_{n\mathbf{k}}u_{n\mathbf{k}}(\mathbf{r}) \tag{2.2.18}$$

and the energy eigenvalue in eq.(2.2.17) near a characteristic point $\mathbf{k}_0$ can be expressed as

$$E_n(\mathbf{k}) = E_n(\mathbf{k}_0) + \frac{\hbar^2(\mathbf{k} - \mathbf{k}_0)^2}{2m_0} + \frac{\hbar^2}{m_0^2}\sum_{l,n}{}' \frac{[(\mathbf{k} - \mathbf{k}_0).\mathbf{M}_{ln}(\mathbf{k}_0)]^2}{E_n(\mathbf{k}_0) - E_l(\mathbf{k}_0)}. \tag{2.2.19}$$

Eq.(2.2.19) can be simplified when interactions between only two bands are of interest (e.g., the valence and conduction bands) and the energy difference between these is small compared to the difference with all other bands. This is exactly the case of

silicon nanostructures where the difference between HOMO-LUMO bands are small enough so that **k.p** perturbation works. Then we can write

$$E_n(\mathbf{k}) = E_n(0) + \frac{\hbar^2}{2}\sum_i^3 \frac{(k_i - k_0)^2}{m_i^*}, \tag{2.2.20}$$

where i=x, y, z and the effective mass can be expressed as

$$\frac{1}{m^*} = \frac{1}{m_0} \pm \frac{2|\mathbf{M}(\mathbf{k}_0)|^2}{m_0^2[E_n(\mathbf{k}_0) - E_l(\mathbf{k}_0)]}, \tag{2.2.21}$$

with +ve or -ve for the upper or lower band, respectively.

One can use eq.(2.2.19) for the deviations of $E(\mathbf{k})$ from parabolicity near a critical point $\mathbf{k}_0$ as

$$E(\mathbf{k} - \mathbf{k}_0) = -\frac{E_g}{2} + \frac{\hbar^2(\mathbf{k} - \mathbf{k}_0)^2}{2m_0} \pm \frac{1}{2}\sqrt{E_g^2 \pm \frac{4\hbar^2(\mathbf{k} - \mathbf{k}_0)^2|M_{nl}(\mathbf{k}_0)|^2}{m_0^2}} \tag{2.2.22}$$

which yields with eq.(2.2.21),

$$E(\mathbf{k} - \mathbf{k}_0) = -\frac{E_g}{2} + \frac{\hbar^2(\mathbf{k} - \mathbf{k}_0)^2}{2m_0} \pm \frac{E_g}{2}\sqrt{1 + \frac{2\hbar^2(\mathbf{k} - \mathbf{k}_0)^2}{E_g}(\frac{1}{m^*} - \frac{1}{m_0})} \tag{2.2.23}$$

with m^* as the effective mass (assumed to be the same in all directions) in the conduction (+) or valence (-) band. $E_g = E_c(\mathbf{k}_0) - E_v(\mathbf{k}_0)$ is the bandgap energy. This illustrates the usefulness of the **k.p** method in a simple example.

Due to the confinement effect however, the band gap is size and geometry dependent. Different calculations show that

$$E_g^{nano} = E_g^{bulk} + \frac{\beta}{d^\gamma}. \tag{2.2.24}$$

where the γ range between 1.2 and 1.8 Proot et al. [21], β is the confinement parameter and 'd' is diameter or effective crystal size. Now the solution for the energy

can be obtained by solving eq.(2.2.21) and eq.(2.2.24) together for different size of the nanoparticles. Depending on the size of the nanoclusters the size dependence of the $E(\mathbf{k} - \mathbf{k}_0)$ can be obtained by taking other parameters from experimental PL spectrum. This was our main concern of this chapter, and we have found out an analytic expression for the band energies using $\mathbf{k}.\mathbf{p}$ perturbation method.

In the next chapter we will exploit optical properties of nano-silicon with the help of optical constants namely the absorption coefficient and dielectric function.

Chapter 3

Calculation of optical absorption coefficient and dielectric function

In this chapter we are going to calculate the linear optical constants, optical absorption coefficient and dielectric function, of direct band gap silicon nanocrystals with the help of optically induced band-to-band transitions. Optically induced transitions are resonance transitions and provide the most direct information about the band structure of semiconductors. These quantities are experimentally measurable one and has paramount applied interest. We will see how **k.p** method is implemented to derive these expressions.

3.1 Optical transition rate and dipole matrix elements

It is inferred via a simple zone-folding argument that nano-sized silicon structures of size below 10nm are approximately direct-gap semiconductors Read et al. [32] and Iyer et al. [33]. One way to convert an indirect semiconductor into a direct one is to form a superlattice (i.e Si and Ge) [34]. In doing so, the size of the Brillouin

zone is reduced and a portion of the conduction band minimum is folded onto the Γ point, resulting in a quasidirect gap system. Therefore, the quantitative descriptions of absorption and luminescence have to take into account the real band structure of nanocrystals because it leads to the shift of optical transition energies and/or to the changing of the optical selection rules [35, 36].

In bulk silicon optical transitions are indirect one because the lowest energy minimum of the conduction band is not at the same $\mathbf{k}$ as the highest maximum of the valence band. For instance the maximum of the valence band is at $\mathbf{k}$=0, but the minimum of the conduction band is at $\mathbf{k} \neq 0$. Direct optical transitions occur when both highest maximum of the valence band and lowest minimum of the conduction band occur at the same $\mathbf{k}$ and identify direct band gap materials. Therefore, we are going to consider direct transitions which involve a direct optical excitation from the valence to the conduction band, using only photons in direct band gap silicon nanocrystallites. Recently there are many investigations where it is observed that quantum confined nano-silicon structures are direct band gap material which show zero phonon transition reflected in the Raman spectra.

Let us consider the interband transitions from the lowest quantum size level of electrons caused by the absorption of linear polarized light of sufficiently short wavelength with

$$\mathbf{A} = A_0 \hat{\mathbf{e}} \exp\left\{ j(\mathbf{k}_0.\mathbf{r} - \omega t) \right\}, \tag{3.1.1}$$

where A_0, $\hat{\mathbf{e}}$ and $\mathbf{k}_0$ are the amplitude, the electric polarization vector and the wave vector of the light travelling in $\mathbf{r}$-direction respectively. Therefore, the dipole matrix

elements are given by

$$\hat{\mathbf{e}}.\mathbf{M}_{\mu\nu}(\mathbf{k}) = \langle\varphi_\mu|\hat{\mathbf{e}}.\mathbf{p}|\varphi_\nu\rangle. \tag{3.1.2}$$

The momentum matrix element can be approximated for transitions from the three valence band gap near E_g from the Kane estimate [37] using

$$|\hat{\mathbf{e}}.\mathbf{M}_{cv}|^2 = (\frac{m_0}{\hbar})^2\mathbf{p}^2, \tag{3.1.3}$$

where $\mathbf{p}$ is the interband (momentum matrix) parameter and its unit is $\frac{Jm}{sec^2}$, which can be obtained from the $\mathbf{k}.\mathbf{p}$ perturbation theory. It is important to mention that Kane estimate is used for other direct gap structures. Kane estimated that

$$\begin{aligned} \mathbf{p}^2 &= \left(\frac{1}{m_e^*} - \frac{1}{m_0}\right)\frac{3}{2}\hbar^2\frac{E_g+\Delta_0}{3E_g+2\Delta_0}E_g \\ &= \frac{3}{2}\hbar^2\left(\frac{m_0-m_e^*}{m_e^*m_0}\right)\frac{E_g+\Delta_0}{3E_g+2\Delta_0}E_g. \end{aligned} \tag{3.1.4}$$

Here Δ_0 , m_e^*, E_g and m_0 are the spin-orbit splitting energy, effective mass of electron in the conduction band, band gap and electron rest mass. With known m_e^*, E_g, and Δ_0, we obtain a numerical value for $\mathbf{p}$, and therefore for the matrix elements

$$|\hat{\mathbf{e}}.\mathbf{M}_{cv}|^2 = \frac{3}{2}\frac{m_0}{m_e^*}(m_0 - m_e^*)\frac{E_g+\Delta_0}{3E_g+2\Delta_0}E_g. \tag{3.1.5}$$

It is already known and established that for nanoclusters the band gap is given by eq.(2.2.24).

For the time-dependent perturbing potential given by

$$V(t) = V(\mathbf{k},\mathbf{r})\exp(-j\omega t), \tag{3.1.6}$$

the famous Fermi Golden Rule is represented by

$$P_{i\to n} = \frac{2\pi}{\hbar}|V_{ni}(\mathbf{k},\mathbf{r})|^2\delta(E_n - E_i - \hbar\omega), \tag{3.1.7}$$

where $V(\mathbf{k}, \mathbf{r})$ is independent of time, n and i are the final state and the initial states of an electron respectively [38]. In our case the perturbing Hamiltonian is

$$\begin{aligned} H_{e-photon} &= -\frac{e}{m_0 c}\mathbf{A}.\mathbf{p} \\ &= \left\{\left(-\frac{eA_0}{m_0 c}\hat{\mathbf{e}}.\mathbf{p}\right)\exp[j\mathbf{k}_0.\mathbf{r}]\right\}\exp(-j\omega t), \end{aligned} \tag{3.1.8}$$

and using electric dipole approximation ($\exp[j\mathbf{k}_0.\mathbf{r}] = 1 + j\mathbf{k}_0.\mathbf{r} + ... \approx 1$). We can rewrite eq.(3.1.8) as follows

$$\begin{aligned} H_{e-photon} &= -\frac{e}{m_0 c}\mathbf{A}.\mathbf{p} \\ &= \left(-\frac{eA_0}{m_0 c}\hat{\mathbf{e}}.\mathbf{p}\right)\exp(-j\omega t) \end{aligned} \tag{3.1.9}$$

The justification for such approximation lies in the fact that the optical effects in nano-silicon is triggered by e-h recombination processes across the band gap. It is therefore, important to look at the coupling of the external radiation with the valence band electron to be able to lift in the conduction band. Hence, the probability of an electron to make a transition from valence band state to conduction band state, $P_{\nu\rightarrow\mu}$, with the help of eq.(3.1.7) is given by

$$P_{\nu\rightarrow\mu} = \frac{2\pi}{\hbar}\left(\frac{eA_0}{m_0 c}\right)^2 |\hat{\mathbf{e}}.\mathbf{M}_{\mu\nu}(\mathbf{k}, \mathbf{r})|^2 \delta(E_\mu - E_\nu - \hbar\omega). \tag{3.1.10}$$

Now after summing over all states and values of $\mathbf{k}$ we get the total number of optically induced transitions per unit volume and unit time which are initiated with the given photon energy ($\hbar\omega$)

$$W(\omega) = \frac{2\pi}{\hbar}(\frac{eA_0}{m_0 c})^2 \sum_{\mu,\nu}\sum_{\mathbf{k}} |\hat{\mathbf{e}}.\mathbf{M}_{\mu\nu}(\mathbf{k})|^2 \delta(E_\mu(\mathbf{k}) - E_\nu(\mathbf{k}) - \hbar\omega). \tag{3.1.11}$$

As can be seen from eq.(3.1.11) the number of optically induced transitions at the same **k** (i.e., neglecting the wavevector of the phonon) between conduction band and valence band is proportional to the square of the momentum matrix elements or the probability P of optical transitions is proportional to the square of matrix element of the operator or dipole matrix element $\hat{\mathbf{e}}.\mathbf{p}$ between the electrons and holes wavefunctions in the conduction band and valence band. This is one of our important result on optical properties of nano-silicon.

3.2 Calculation of linear optical absorption

To obtain the absorption coefficient for a particular nanocrystallite having definite size as a function of incident photon energy, sophisticated silicon cluster calculations are needed. We, however, are only interested in its form near the band edge. Fortunately, this considerably simplifies the calculation by an effective-mass approach which as we shall see, still describes the essential physics of the absorption mechanism for silicon nanocrystals up to nearly 1 eV beyond the band edge. Nano-sized silicon structures which are approximately direct-gap still have three-dimensional continuum of states with energies above that of the local (upshifted) bandgap. The resulting local density of states near the new band edge will therefore arise from a quasi-three-dimensional system and will not be that different from the usual square root law of the three-dimensional continuum [35]. Without the dynamical aspects of quantum confinement, the zone-folding argument implies that the dominant absorption mechanism at the band edge would be "direct allowed" as in GaAs [35].

For very small (smaller than average) crystallites (typically 2-4 nm) the assumption of a continuum of states may be invalid or weakened. Indeed a discrete energy spectrum is expected. Such crystallites would not contribute significantly to the band-edge absorption because it is the larger than average crystallites (typically 6-10 nm) that dominate the band edge [35]. In addition, experiment does not seem to show any discrete structure although, the instrumental function of the apparatus may not resolve such structure. Therefore, we are going to examine the absorption coefficient of the silicon nanocrystals (typically 6-10 nm) as a function of photon energy and band gap for pure as well as when passivated by hydrogen and oxygen. In addition to the direct-gap nature of the crystallites, the lack of translational invariance removes the requirement for momentum conservation, giving an absorption mechanism quite different from that of the bulk silicon case [35, 36, 42].

The optical absorption coefficient is proportional to the number of optical transitions per unit volume and time elements [29]. Therefore, the optical absorption coefficient can be calculated from simple optical principles [39]. It is given by the absorbed energy per unit time, $\hbar\omega W(\omega)$, divided by the energy flux, $\frac{A_0^2\omega^2\varepsilon_0 n_r}{2\pi c}$, i.e

$$\alpha(\omega) = \frac{\hbar\omega W(\omega)}{A_0^2\omega^2\varepsilon_0 n_r/(2\pi c)}. \tag{3.2.1}$$

The energy flux is equal to optical energy density given by the square of the wave amplitude per wavelength interval, $\frac{A_0^2\omega^2 n_r^2}{2\pi c^2}$, divided by the light velocity within the semiconductor, i.e $\frac{c}{n_r}$. With the help of the eq.(3.1.11) and eq.(3.2.1), we now obtain the optical absorption coefficient

$$\alpha(\omega) = \frac{4\pi^2 e^2}{\varepsilon_0 n_r c m_0^2 \omega} \sum_{\mu,\nu} \sum_{\mathbf{k}} |\hat{\mathbf{e}}.\mathbf{M}_{\mu\nu}(\mathbf{k})|^2 \delta(E_\mu(\mathbf{k}) - E_\nu(\mathbf{k}) - \hbar\omega). \tag{3.2.2}$$

As far as optical properties of semiconductor nanocrystallites are concerned this is an important parameter which experimentalists are interested in. This parameter is used for optical application of semiconductor nano-material for photonic and optoelectronic devices.

3.2.1 The fundamental absorption edge and joint density of states

Absorption of a photon in a material corresponds to an optical transition of one electron from the ground state (valence band) to the excited state (conduction band) [29]. The transition, in fact, generates two oppositely charged carriers, since simultaneously a hole is created in the valence band. The two elementary charges physically emerge at the same part in space within the crystal.

Attention will now be focused on the energy range near the threshold for valence-to-conduction band transitions, the fundamental absorption edge ($k \approx 0$). Usually, several excitation processes are possible between different subbands for a given optical excitation energy. For photon energy slightly exceeding the band gap, transitions between the different valence bands into different E(k) values of the conduction band are possible near k=0.

The summation over $\mathbf{k}$ in eq.(3.2.2) identifies the sum over all possible transitions which can be initiated by photons with a certain energy $\hbar\omega$, and it is commonly referred to as the **joint density of states** between these two bands [29]. Therefore, to study the direct optical absorption edge further as a function of photon energy and band gap energy we need to calculate the joint density of states between the

valence and conduction band states (HOMO and LUMO states). In a similar fashion discussed for density of states in section one of chapter two under the assumption of parabolic band generally the joint density of states between the valence state and conduction band state is given by

$$\begin{aligned} J_{\mu\nu}(\omega) &= \sum_{\mathbf{k}} \delta(E_\mu(\mathbf{k}) - E_\nu(\mathbf{k}) - \hbar\omega) \\ &= \frac{2}{(2\pi)^D} \int \delta\left(E_\mu(\mathbf{k}) - E_\nu(\mathbf{k}) - \hbar\omega\right) d\mathbf{k}, \end{aligned} \tag{3.2.3}$$

where D=1, 2 and 3 is the number of dimensions quantum wire, quantum well and three dimensional structure of a direct band semiconductor. The joint density of states of the transition between the top of one valence band to the bottom of the lowest conduction band when both lie at k=0 estimated from a parabolic approximation of both band for direct band silicon nanocrystals can also be written as,

$$J_{\mu\nu} = \frac{2}{(2\pi)^3} \frac{d\left(\frac{4\pi}{3}k^3\right)}{d(\hbar\omega)}. \tag{3.2.4}$$

The transition between the top of one valence band to the bottom of the lowest of the conduction band when both lie at k=0 is responsible for the direct optical absorption edge. The joint density of states is estimated from a parabolic approximation of both bands as,

$$\begin{aligned} \hbar\omega &= E_c(\mathbf{k}) - E_v(\mathbf{k}) \\ &= E_g + \frac{\hbar^2 k^2}{2m_e^*} + \frac{\hbar^2 k^2}{2m_h^*} \\ &= E_g + \frac{\hbar^2 k^2}{2m_r^*}, \end{aligned} \tag{3.2.5}$$

and

$$\frac{1}{m_r^*} = \frac{1}{m_e^*} + \frac{1}{m_h^*}, \tag{3.2.6}$$

where m_r^*, m_e^* , m_h^* and E_g being the reduced mass, effective mass of electron, effective mass of hole and band gap of silicon nanocrystal respectively.

Solving for k from eq.(3.2.5) and substituting back in eq.(3.2.4) we get the expression for the joint density of states as

$$J_{cv} = \frac{1}{2\pi^2}\left(\frac{2m_r^*}{\hbar^2}\right)^{3/2}\sqrt{\hbar\omega - E_g}. \tag{3.2.7}$$

Using eqs.(3.2.3, 3.2.4, 3.2.7), we obtain the expression for the optical absorption co-efficient near the band edge,

$$\begin{aligned}
\alpha(\omega) &= \frac{4\pi^2 e^2}{\varepsilon_0 n c m_0^2 \omega}\sum_{\mathbf{k}} |\hat{\mathbf{e}}.\mathbf{M}_{\mu\nu}(\mathbf{k})|^2 \delta(E_\mu(\mathbf{k}) - E_\nu(\mathbf{k}) - \hbar\omega) \\
&= \frac{4\pi^2 e^2}{\varepsilon_0 n c m_0^2 \omega}\left[|\hat{\mathbf{e}}.M_{cv}|^2 J_{cv}\right] \\
&= \frac{4\pi^2 e^2}{\varepsilon_0 n c m_0^2 \omega}|\hat{\mathbf{e}}.M_{cv}|^2\left[\frac{1}{2\pi^2}\left(\frac{2m_r^*}{\hbar^2}\right)^{3/2}\sqrt{\hbar\omega - E_g}\right] \\
&= \left(\frac{2e^2(2m_r^*)^{3/2}}{\varepsilon_0 n_r c m_0^2 \hbar^3 \omega}\right)|\hat{\mathbf{e}}.M_{cv}|^2\sqrt{\hbar\omega - E_g}.
\end{aligned} \tag{3.2.8}$$

After introducing the value of $\hat{\mathbf{e}}.M_{cv}$ from eq.(3.1.5) into eq.(3.2.8), we get optical absorption co-efficient near the band edge as ([40] using Kane approximation)

$$\begin{aligned}
\alpha(\omega) &= \frac{3e^2(2m_r^*)^{3/2}}{\varepsilon_0 n_r c m_0 \hbar^2}\left(\frac{m_0 - m_e^*}{m_e^*}\right)\frac{E_g + \Delta_0}{3E_g + 2\Delta_0}\frac{E_g}{\hbar\omega}\sqrt{\hbar\omega - E_g} \\
&= \frac{3e^2\sqrt{m_0}}{\varepsilon_0 n_r \hbar^2 c}\left(\frac{2m_r^*}{m_0}\right)^{\frac{3}{2}}\frac{m_0 - m_e^*}{m_e^*}\frac{E_g + \Delta_0}{3E_g + 2\Delta_0}\frac{E_g}{\hbar\omega}\sqrt{\hbar\omega - E_g}.
\end{aligned} \tag{3.2.9}$$

For $\hbar\omega \simeq E_g$ i.e the photoluminescence occurs in the visible range so that $\omega \simeq 2\pi \times 10^{16} sec^{-1}$,

$$\begin{aligned}
\alpha(\omega) &= \frac{3e^2\sqrt{m_0}}{\varepsilon_0 n_r \hbar^2 c}\left(\frac{2m_e^* m_h^*}{m_0(m_e^*+m_h^*)}\right)^{\frac{3}{2}}\frac{m_0-m_n}{m_n}f(E_g)\\
&= \frac{3e^2\sqrt{m_0}}{\varepsilon_0 n_r \hbar^2 c}\left(\frac{2m_r^*}{m_0}\right)^{\frac{3}{2}}\frac{m_0-m_e^*}{m_e^*}f(E_g)\\
&= 3.322\times 10^6 \times \left(\frac{2m_r^*}{m_0}\right)^{\frac{3}{2}}\left(\frac{3}{n_r}\right)\frac{m_0-m_e^*}{m_e^*}f(E_g)\ eV^{-1/2}cm^{-1}, \quad (3.2.10)
\end{aligned}$$

with

$$f(E_g) = \frac{E_g+\Delta_0}{3E_g+2\Delta_0}\sqrt{\hbar\omega - E_g}. \quad (3.2.11)$$

is proportional to the square root of the energy difference from the band edge.

So far we have seen how the optical absorption coefficient near the band edge of direct band gap silicon nanocrystals is related to the band gap and photon energy which indirectly related to silicon nanocrystal size. In the next section we are going to see how the imaginary part of the dielectric function of silicon nanocrystals is related to energy gap, photon energy and the silicon nanocrystal size. The optical nature of the band gap is reflected in the dielectric response function.

3.3 Dielectric function

The study of the dielectric function via the optical transition matrix elements to obtain information directly on absorption and photoluminescence spectra, have direct applied interest.

Because the evaluation of the imaginary part of the dielectric function $\varepsilon_2(\omega)$ is directly performed through calculation of the dipole matrix elements for a quantum

dot, it can also allow us to get information indirectly on the relevant radiative PL processes looking at the features of $\varepsilon_2(\omega)$, containing the various inter-band transitions, weighted by the momentum optical matrix element. The luminescence intensity is related through an energy balance relation to the absorption coefficient, which is directly linked to the imaginary part of the dielectric function. The real part of the dielectric function can be calculated using Kramers Kronig relations

$$\varepsilon_1(\omega) = 1 + \frac{2}{\pi}\wp \int_0^\infty \frac{\omega' \varepsilon_2(\omega') d\omega'}{\omega'^2 - \omega^2} \tag{3.3.1}$$

where $\wp$ represents the Cauchy principal value of the integral (omitting the contribution to the integral of the singularity at $\omega = \omega'$). The luminescence intensity $I_{PL}(\omega)$ is related to the absorption coefficient $\alpha(\omega)$ and imaginary part of the dielectric function through the energy balance relation [41] as follows

$$I_{PL}(\omega) \sim \alpha(\omega) f(\omega) \sim \omega \epsilon_2(\omega) f(\omega) \tag{3.3.2}$$

where $f(\omega)$ is a suitable thermal function.

A slightly different method to our absorption model has been employed by [42, 43] to determine the dielectric function of crystalline nano-sized silicon structures beginning with the bulk silicon Bloch wavefunctions the so called envelope approximation. Here, the wavefunction for a given band is a weighted sum of all the Bloch wavefunctions of that band. This has the advantage that the bulk silicon absorption coefficient is recovered for large crystallites. We need not consider this sophistication because the typical crystallite sizes that we consider fall well within the quantum regime-having diameters less than 10 nm-where the zone-folding argument is expected to hold.

We know that the imaginary part of the dielectric function is directly related to the absorption coefficient and refractive index by the relation

$$\varepsilon_2 = \frac{\alpha n_r c}{\omega}, \tag{3.3.3}$$

with help of eq.(3.2.2) and eq.(3.3.3) we get

$$\varepsilon_2(\omega) = \frac{4\pi^2 e^2}{\varepsilon_0 m_0^2 \omega^2} \sum_{\mu,\nu} \sum_{\mathbf{k}} |\hat{\mathbf{e}}.\mathbf{M}_{eh}(\mathbf{k})|^2 \delta(E_\mu(\mathbf{k}) - E_\nu(\mathbf{k}) - \hbar\omega). \tag{3.3.4}$$

Hence, from eq.(3.2.9) and eq.(3.3.3)the imaginary part of the dielectric function of a silicon nanocrystal near the band edge in terms of silicon nanocrystal band gap and photon frequency is given by

$$\begin{aligned} \varepsilon_2(\omega) &= \frac{3e^2(2m_r^*)^{3/2}}{\varepsilon_0 m_0 \omega \hbar^2} \left(\frac{m_0 - m_e^*}{m_e^*}\right) \frac{E_g + \Delta_0}{3E_g + 2\Delta_0} \frac{E_g}{\hbar\omega} \sqrt{\hbar\omega - E_g} \\ &= \frac{3e^2\sqrt{m_0}}{\varepsilon_0 \omega \hbar^2} \left(\frac{2m_r^*}{m_0}\right)^{3/2} \left(\frac{m_0 - m_e^*}{m_e^*}\right) \frac{E_g + \Delta_0}{3E_g + 2\Delta_0} \frac{E_g}{\hbar\omega} \sqrt{\hbar\omega - E_g}. \end{aligned} \tag{3.3.5}$$

Finally, for $\hbar\omega \simeq E_g$ i.e the photoluminescence occurs in the visible range so that $\omega \simeq 2\pi \times 10^{16} sec^{-1}$ and introducing eq.(3.2.11), we can write eq.(3.3.5) as follows,

$$\begin{aligned} \varepsilon_2(\omega) &= \frac{3e^2\sqrt{m_0}}{\varepsilon_0 \omega \hbar^2} \left(\frac{2m_r^*}{m_0}\right)^{3/2} \left(\frac{m_0 - m_e^*}{m_e^*}\right) \frac{E_g + \Delta_0}{3E_g + 2\Delta_0} \sqrt{\hbar\omega - E_g} \\ &= \frac{3e^2\sqrt{m_0}}{\varepsilon_0 \omega \hbar^2} \left(\frac{2m_r^*}{m_0}\right)^{3/2} \left(\frac{m_0 - m_e^*}{m_e^*}\right) f(E_g) \\ &= 1.97 \times 10^2 \times \left(\frac{2m_r^*}{m_0}\right)^{3/2} \left(\frac{m_0 - m_e^*}{m_e^*}\right) \frac{f(E_g)}{\hbar\omega}\ eV^{1/2}. \end{aligned} \tag{3.3.6}$$

Calculation of the optical properties of nanostructures performed through the evaluation of dielectric function is more advantageous than through absorption coefficient because it does not involve another optical constant refractive index of the material in its expression.

Chapter 4

Results and Discussions

In the last chapter we have seen how the optical absorption coefficient and the dielectric function are related to the band gap energy and photon energy using Kane estimate of the dipole matrix elements for direct band gap. Now we want to see how both the optical absorption coefficient and the imaginary part of the dielectric function depend on size of the silicon nanocrystallites. To find the relationship between optical absorption coefficient and the dielectric function with size of direct band gap silicon nanocrystals it is important to look at how the energy band gap varies as a function of nanocrystallite size. In order to estimate the variation of the HOMO-LUMO gap with the size one has to simulate the size dependent the band structure of the nanoparticles and then fit the data with an empirical law. This has been done repeatedly for example in the case of silicon, zinc oxide, CdSe or CuBr [44]. Interestingly, for all these materials, the variation is observed to follow roughly the same kind of law,

$$E_g(d) = E_{g0} + \frac{\beta}{d^\gamma} \tag{4.0.1}$$

with the same γ exponent, $\gamma \sim 1.4$. The values of β and γ depend on the nature of the surface as well as size and symmetry of nanoclusters. Zunger et al. [45] using

tight-binding method, Tripathy et al. [46] and Ghoshal et al. [47] using local pseudopotential method calculated the band gap energy as a function of diameter (size) for clean surface silicon nanoclusters at room temperature and found approximately the gap as

$$E_g^{nano}(d) = E_{g0}^{bulk} + \frac{3.73}{d^{1.37}} \ (eV), \tag{4.0.2}$$

where $E_g^{nano}(d)$, $E_{g0}^{bulk}(d)$ and 'd in (nm)' are the band gap energy of silicon nanocrystal, bulk silicon band gap energy at room temperature and diameter (size) of the silicon nanocrystallite respectively. Similarly, Tripathy et al. [37] also calculated band gap energy for hydrogen passivated silicon nanocrystals using local pseudopotential method at room temperature as

$$E_g(d) = E_{g0} + \frac{4.042}{d^{1.353}} \ (eV). \tag{4.0.3}$$

Comparing eq.(4.0.2) and eq.(4.0.3) we can see besides the quantum confinement, surface passivation play important role and increase the band gap of the nanocrystals. Therefore, surface passivation also affects the photonic and optoelectronic properties of nanocrystals by enhancing the HOMO-LUMO gap.

Taking effective mass of hole, $m_h^* = 0.54m_0$, effective mass of electron, $m_e^* = 0.40m_0$ [42], bulk silicon spin-orbit splitting, $\Delta_0 = 0.044 \ eV$ [29] and effective refractive index of silicon nanocrystallite, $n_r = 1.7$ [11] we can finally get the optical absorption coefficient for silicon nanoclusters (6-10nm) from eq.(3.2.9) as

$$\alpha(\omega) = 2.744 \times 10^6 \times \left(\frac{E_g}{\hbar\omega}\right)\left(\frac{E_g + 0.044}{3E_g + 0.088}\right)\sqrt{\hbar\omega - E_g} \ eV^{-1/2}cm^{-1}, \tag{4.0.4}$$

and similarly the imaginary part of the dielectric function from eq.(3.3.5) become

$$\varepsilon_2(\omega) = 92 \times \left(\frac{E_g}{\hbar\omega}\right)\left(\frac{E_g + 0.044}{3E_g + 0.088}\right)\frac{\sqrt{\hbar\omega - E_g}}{\hbar\omega} \ eV^{1/2}. \tag{4.0.5}$$

Hence, eq.(4.0.4) and eq.(4.0.5) explicit function of photon energy and band gap energy but implicit function of silicon nanoclusters size through band gap energy.

Therefore, with the help of eqs.(4.0.2-4.0.4) we get the variation of the optical absorption coefficient near the band edge as a function of effective sizes (6-10nm) for clean and hydrogen passivated surface silicon nanoclusters at a given frequency is shown in figure (4.1). The variation of the optical absorption coefficient near the band edge as a function of photon energy for clean and hydrogen passivated surface silicon nanoclusters of effective size (8nm) is depicted in figure (4.2).

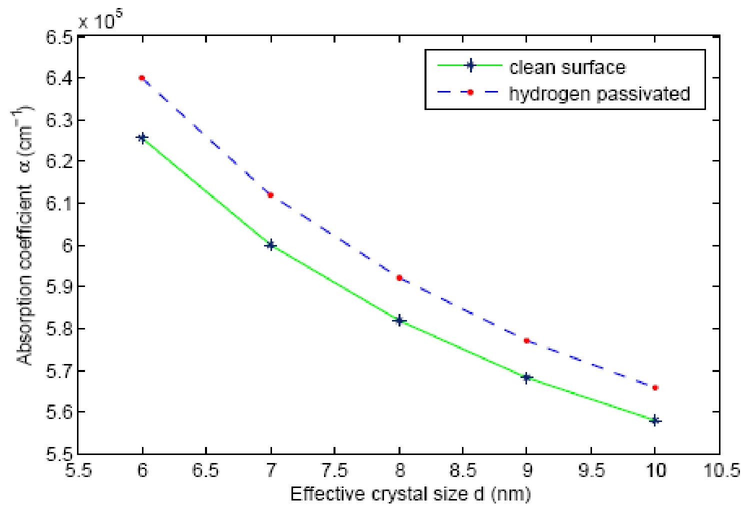

Figure 4.1: *Optical absorption coefficient as a function of silicon nanocluster size for photon energy* $\hbar\omega$*=2.2 eV.*

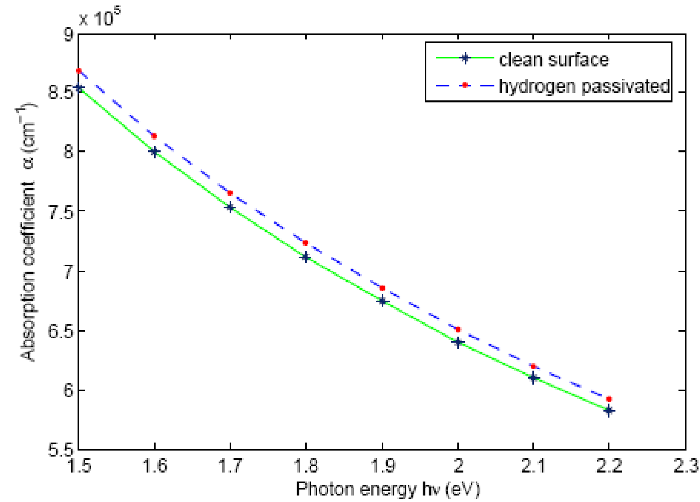

Figure 4.2: *Optical absorption coefficient as a function of photon energy for effective silicon nanocluster size d=8nm.*

Finally, with the help of eqs.(4.0.2-4.0.3) and eq.(4.0.5) the variation of the imaginary part of the dielectric function near the band edge as a function of effective sizes (6-10nm) for clean and hydrogen passivated surface silicon nanoclusters at a given frequency is shown in figure (4.3). The variation of the imaginary part of the dielectric function near the band edge versus photon energy for clean and hydrogen passivated surface of silicon nanoclusters of effective size (8nm) is represented in figure (4.4).

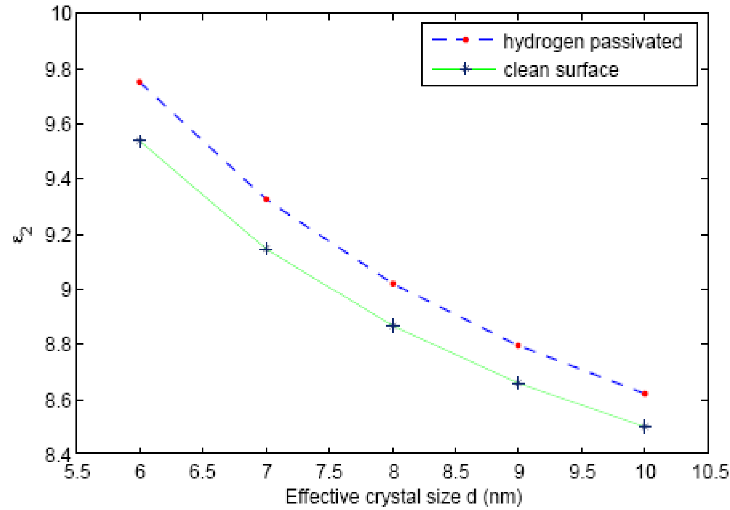

Figure 4.3: *Imaginary part of the dielectric function as a function of silicon nanocluster size for photon energy* $\hbar\omega$=*2.2 eV.*

From the figures (4.1-4.4) we can observe both the optical absorption coefficient and imaginary part of the dielectric function near the band edge of silicon nanoclusters for clean as well as hydrogen passivated surfaces having effective size d (6-10nm) decrease with the increase of photon energy and effective cluster size. This is because of the quantum confinement effect which causes an increase in the energy gap and transition from indirect to direct band gap. For nanocluster effective size approximately below and equal to 10nm and especially for (6-10nm) the density of states changes with size. It is clearly seen from the graphs of both optical absorption coefficient and imaginary part of the dielectric function near the band edge that the hydrogen passivated silicon nanoclusters having effective size (6-10nm) lie above unpassivated clusters. Knowing the dependence of optical absorption coefficient and imaginary part of the dielectric function on the photon and cluster size will help us to get information about the

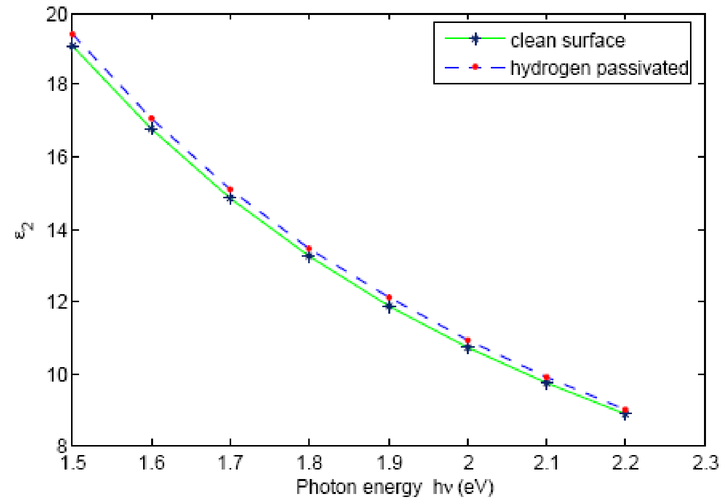

Figure 4.4: *Imaginary part of the dielectric function as a function of photon energy for effective silicon nanocluster size d=8nm.*

relationship absorption and photoluminescence spectra. In the recent years this is observed in different experiments and simulations and our result is in conformity with other observations [15], [35], [48] and [49].

Chapter 5

Summary and Conclusion

In the thesis our main aim was to investigate analytically the optical properties of nano-silicon. It is important for photonic and optoelectronic applications. Bulk silicon is poor emitter of light, while silicon nanostructures (porous silicon, quantum dots, quantum wells and nanoclusters), exhibit strong photoluminescence at room temperature which is observed only after a drastic reduction of silicon size and has been related to quantum confinement effect. Quantum confinement effect widens the band gap that occurs when the nanostructures size become comparable to the Bohr exciton radius in bulk silicon.

Silicon nanostructures have tremendous applications in the photoluminescence, optoelectronic and photonic devices. They can be easily integrated into silicon wafer processing and utilized for biological, chemical, optical sensors and memory devices. It has been discussed that silicon nanostructures can be fabricated by different methods. The most common ones are electrochemical anodization of bulk silicon in an HF electrolyte, plasma enhanced chemical vapor deposition (PECVD), ion-implantation.

Optical properties of nano-silicon is affected by quantum confinement effect, and by the enhanced role of states- and defect- at the surface (surface passivation). Quantum confinement effect change the indirect band gap nature of bulk silicon to direct band gap in the nano-silicon whose average size is below and equal to 10nm. Although quantum confinement alone cannot explain the whole physics of silicon nanostructures but gives explanation of the observation of luminescence.

In order to characterize the physical properties like optical transitions in silicon nanostructures, the information about the density of states which depends on the dimensionality of the system is very crucial. We have seen how **k.p** perturbation method works for silicon nanostructures which become direct band gap due to quantum confinement effect. With the help of Kane approximation of momentum matrix element of direct band gap semiconductors we obtain the dipole matrix element. Together with knowledge of joint density of states between valence and conduction band states which help us to calculate the optical absorption coefficient and imaginary part of the dielectric function near the band edge for silicon nanocrystals whose effective size is in between (6-10nm). These parameters provide information directly on absorption and photoluminescence spectra.

After demonstrating the dependence of band gap as a function of the effective nanocluster size we found out the variations of optical absorption coefficient and imaginary part of the dielectric function near the band edge with crystal size and photon energy for silicon nanoclusters for both clean and hydrogenated surface (6-10nm) obtained from the modified joint density of states, confinement and surface effects on the silicon nanocluster. The primary interest was to examine size dependent optical

absorption coefficient and dielectric function as a function of photon energy. Our theory are in qualitative agreement with other observations.

We have concluded that quantum confinement effects and surface passivation increase the optical absorption coefficient and dielectric function of the nano-silicon with decreasing size of the nanocluster. The luminescence intensity $I_{PL}(\omega)$ is directly related to the optical absorption coefficient $\alpha(\omega)$ or to the imaginary part of the dielectric function [41]. Therefore, the photoluminescence intensity increase with decreasing size of the nanocluster for silicon nanocluster whose effective size (6-10nm) as observed by many experiment are in conformity with our work. However, there are many other important issues, for example temperature and geometry dependent α, ε, exciton binding energy, oscillator strength etc. can also be dealt with the help of this theory with suitable modification [50].

Bibliography

[1] A. Uhlir, Bell Syst. Tech. **35**, 333 (1956).

[2] S. Limaye, S. Subramanian, B. Goller, J. Diener, and D. Kovalev, Phys. Stat. Sol. (a) **204**, 1297 (2007).

[3] S. Botti, M. L. Terranova, V. Sessa, S. Piccirillo and M. Rossi, Appl. Organometal. Chem. **15**, 388 (2001).

[4] M. Ehbrecht, B. Kohn, F. Huisken, M. A. Laguna, V. Paillard, Phys. Rev. B **56**, 6958 (1997).

[5] C. Delerue, G. Allan, M. Lannoo, Phys. Rev. B **48**, 11024 (1993).

[6] Y. Kanemitsu, H. Huto, Y. Masumoto, T. Fugati, H. Mimura, Phys. Rev. B **48**, 2827 (1993).

[7] Y. Kanemitsu, N. Shimizu, T. Komoda, P. Hemment, B. Sealey, Phys. Rev. B **54**, 14329 (1996) and references cited therein.

[8] A. Polman in Silicon-based Photonics, European Materials Research Society Meeting 2006, Nice, France; M. Fujii et al., Appl. Phys. Lett. **71**, 1198 (1997).

[9] D. Kovalev, E. Gross, N. Knzner, F. Koch, V. Yu. Timoshenko, and M. Fujii, Phys. Rev. Lett. **89**, 137401 (2002).

[10] D. Kovalev, V. Yu. Timoshenko, N. Knzner, E. Gross, and F. Koch, Phys. Rev. Lett. **87**, 68301 (2001).

[11] P. Bettotti, M. Cazzanelli, L. Dal Negro, B. Danese, Z. Gaburro, C. J. Oton, G. Vijaya Prakash and L. Pavesi, J. Phys,: Condens. Matter **14**, 8253 (2002).

[12] X. Badel in Electrochemically etched pore arrays in silicon for X-ray imaging detectors, Ph.D. thesis, KTH, Stockholm, Sweden, 2005.

[13] A. G. Cullis, L. T. Canham, and P. D. J. Calcott, J. Appl. Phys., **82**, 909 (1997).

[14] Tae-Youb Kim, Nae-Man Park, Kyung-Hyun Kim, Young-Woo Ok, Tae-Yeon Seong, Cheo- Jong Choi and Gun Yong Sung, Mat. Res. Soc. Symp. Proc. Vol. **817**, 78 (2004).

[15] D. Kovalev, H. Heckler, G. Polisski, and F. Koch, Phys. Stat. Sol. (a) **215**, 871 (1999).

[16] Lorenzo Pavesi, David Lockwood, Silicon-based Photonics, Appl. Phys. vol. **94** (Springer-Verlag, Berlin 2004).

[17] S. Schuppler et al, Phys. Rev. Lett. **72**, 2648 (1994).

[18] T. van Buuren, L. N. Dinh, L. L. Chase, W. J. Siekhaus, and L. J. Terminello, Phys. Rev. Lett. **80**, 3803 (1998).

[19] M. V. Wolkin, J. Jorne, and P. M. Fauchet, G. Allan, and C. Delerue, Phys. Rev. Lett. **82**, 197 (1999).

[20] L. T. Canham, Appl. Phys. Lett. **57**, 1046 (1990).

[21] J. P. Proot, C. Delerue, and G. Allan, Appl. Phys. Lett. **61**, 1948 (1992).

[22] A. Puzder, A. J. Williamson, J. C. Grossman, and G. Galli, Phys. Rev. Lett. **88**, 97401 (2002).

[23] M. Murayama and T. Nakayama, Phys. Rev. B **49**, 5737 (1994); **52**, 4986 (1995).

[24] G. Vijaya Prakash, M. Cazzanelli, Z. Gaburro, and L. Pavesi, J. Appl. Phys. **91**, 7 (2002).

[25] S. Schmitt-Rink, D. A. B. Miller, and D. S. Chemla, Phys. Rev. B **35**, 8113 (1987).

[26] E. Hanamura, Phys. Rev. B **37**, 1273 (1988).

[27] D. Cotter, M. G. Burt, and R. J. Manning, Phys. Rev. Lett. **68**, 1200 (1992).

[28] J. I. Pankove, Optical Processes in Semiconductors, Prentice-Hall, Englewood Cliffs, New Jersey, 1971.

[29] Karl W. Böer, Survey of Semiconductor Physics: Electrons and Other Particles in Bulk Semiconductors, Nostrand Reinhold, 1990.

[30] Jasprit Singh: www.eecs.umich.edu/∼singh, John-Wiley, 2001.

[31] P. K. Basu, Theory of Optical Processes in Semiconductors: Bulk and Microstructures, Oxford University Press, Oxford, England, 1997.

[32] A. J. Read, R. Needs, K. I. Nash , L. T. Canham , P. D. J. Calcott and A. Qtelsh, Phys. Rev. Lett. **69**, 1232 (1992).

[33] S. Iyer and Y. Xie, Science **260**, 40 (1993).

[34] T. P. Pearsall, J. Bevk, L. C. Feldman, et al., Phys. Rev. Lett. **58**, 729 (1987).

[35] P. M. Derlet, T. C. Choy and A. M. Stoneham, J. Phys.: Condensed. Matter **7**, 2507 (1995).

[36] S. Ossicini, Optical Properties of Confined Silicon Structures, Phys. Stat. Sol. (a) **170**, 377 (1998).

[37] E. O. Kane, J. Phys. Chem. Solids **1**, 245 (1957).

[38] J. J. Sakurai, Modern Quantum Mechanics, Addison-Wesley, 1994.

[39] G. F. Bassani and G. Pastori Parravicini, Electronic States and Optical Transitions in Solid, Pergoman Press, Oxford and New York, 1975.

[40] T. S. Moss, G. T. Burrell and B. Ellis, Semiconductor Optoelectronics, John Wiley and Sons, New York (1973).

[41] L. Dorigoni, O. Bisi, F. Bernardini, and S. Ossicini, Phys. Rev. B **53**, 4557 (1996).

[42] M. Hybertsen, Phys. Rev. lett. **72**, 1514 (1994).

[43] Y. Xie, M. S. Hybemen, W. L. Wilson, S. A. lpri, G. E. Cnver , W. L. Brown , E. Dons, B. E. Weir , A. R. Konan , G. P. Watson and A. Liddle, J. Phys. Rev. B **49**, 5386 (1994).

[44] B. Mercier, G. Ledoux, C. Dujardin, LPCML CNRS UMR 5620, Universite Claude Bernard Lyon I, **10** rue A. M. Amp‘ere, F-69622 Villeurbanne Cedex,

France, Universite de Lyon; D. Nicolas, B. Masenelli, P. Melinon, LPMCN CNRS UMR 5586, Universite Claude Bernard Lyon I, **6** rue A. M. Amp‘ere, F-69622 Villeurbanne Cedex, France, Universite de Lyon and G. Bergeret, IRC CNRS UPR 5401, **2** rue A. Einstein, F-69626 Villeurbanne Cedex, France (January 29, 2007).

[45] A. Zunger, L-W. Wang, Applied Surface Science **102**, 350 (1996).

[46] S. Tripathy, R. K. Soni, S. K. Ghoshal and K. P. Jain, Bull. Matter. Sci., Vol. **24**, 285 (2001).

[47] S. K. Ghoshal, Asian. J. Spect **7**, 49 (2003).

[48] N. Künzner, D. Kovalev, J. Diener, H. Heckler, G. Polisski and F. Koch, Phys. Stat. Sol. (a) **182**, 379 (2000)

[49] B. Delley and E. F. Steigmeier, Phys. Rev. B **47**, 1397 (1993).

[50] H. Gebrehiwet and S. K. Ghoshal (in preparation, 2007).